ELSEVIER

Nuclear Instruments and Methods in Physics Research B 196 (2002) 340–348

NIM B
Beam Interactions with Materials & Atoms

www.elsevier.com/locate/nimb

Precision measurements of gas refractivity by means of a Fabry–Perot interferometer illustrated by the monitoring of radiator refractivity in the DELPHI RICH detectors

T.A. Filippas [a], E. Fokitis [a,*], S. Maltezos [a], K. Patrinos [a], M. Davenport [b]

[a] *Physics Department, National Technical University of Athens, Zografou Campus, GR-157 80 Athens, Greece*
[b] *CERN, EP Division, CH-1211 Geneva 23, Switzerland*

Received 1 January 2002; received in revised form 18 June 2002

Abstract

With an updated, flexible, highly efficient and easily installed system we obtained accurate refractivity $(n-1)$ values. This system is a refractometer based on a Fabry–Perot interferometer and was used to monitor the refractivity of DELPHI RICH Cherenkov radiators near the VUV region. By using a Pt–Ne spectral lamp and improved alignment and temperature control, the refractivities of C_5F_{12} and C_4F_{10} have been monitored since 1996. With this light source, selected to have large coherence lengths, we can extract the refractivity at several wavelengths from one data set only. The estimated errors of the refractivity measurements are less than 1.2%, and depend on wavelength and the type of gas used. The various parameters affecting the accuracy of the refractometer are also discussed. Finally, results from special sample refractivity measurements of the liquid radiator (C_6F_{14}) in its gas phase, are presented.

1. Introduction

The Rich Imaging Technique was first proposed by Seguinot and Ypsilantis [1]. The RICH detectors, in the LEP accelerator DELPHI experiment at CERN, allows for charged particle identification up to momentum values, which depend on the accuracy by which the refractive index, Cherenkov angle and particle momentum are measured. Therefore, accurate values of the refractive index near the vacuum UV range (around 190–200 nm), which is the window of sensitivity of these detectors, is of significant importance. In addition, obtaining the dispersion in a wider spectral range is useful for analysing the Cherenkov rings.

A Fabry–Perot based pressure tunable refractometer, installed in the DELPHI RICH detector area [2], has been used to make it a routine refractivity monitoring device for both gas radiators of RICH, i.e. fluorocarbons C_5F_{12} and C_4F_{10}.

Recent improvements of the refractometer, and the experimental procedure for measuring a gas sample are presented in Section 2. A brief description of the method for analysing the data is presented in Section 3, while the experimental errors are discussed in Section 4. The experimental results, along with the dispersion curves, the

* Corresponding author. Tel.: +30-1-772-3014; fax: +30-1-772-3021.
E-mail address: fokitis@central.ntua.gr (E. Fokitis).

0168-583X/02/$ - see front matter
PII: S0168-583X(02)01291-0

evolution of refractivity during the monitoring period, the measurements of the liquid radiator in its gas phase and the determination from the data of the nitrogen mixing percentage inside the gas radiator are presented in Section 5. The conclusions on the refractivity monitoring performance and the prospects are discussed in the last Section 6.

2. Experimental setup

2.1. Construction of the refractometer

The principle of operation of Fabry–Perot interferometer is described in great details in [3]. Such an instrument consisting of a pressure tunable Fabry–Perot interferometer, was developed to measure the refractivity of gas radiators of RICH detectors in extended spectral range near the VUV [4,5]. This system, operating as a gas refractometer, used as a light source a pen-ray-type low pressure spectral lamp of Hg with Ne carrier gas. Thus, the necessity to operate such an instrument in the environment of the DELPHI experimental area, in order to monitor the variations of the refractivity of the gas radiators of the RICH detectors, posed a number of strict conditions; limited available space, risk of deterioration of the sharpness of the interference fringe patterns due to nearby mechanical vibrations. Two additional conditions were the need of stable optical alignment of the interferometer and the increased level of automation in order to minimize the length of measurement time and the presence of the operator of the refractometer. Therefore, several significant improvements, described briefly below, were implemented.

I A specific mechanical support of the Fabry–Perot etalon, based on the kinematic mount aiming at suppressing the effects of mechanical vibrations in the environment of the interferometer.
II A 1-inch diameter Pt–Ne hollow cathode discharge lamp replaced the Hg–Ne.
III Mechanical improvements in the collimators and the light detection system implemented to assure higher stability and alignment.
IV A proper combination of the spectral lamp and an optical filter with partial suppression of the higher wavelength lines was used in order that the spectral range of interest can be recorded. This was accomplished by using a 0.5 mm pinhole in front of the photomultiplier tube (PMT), which was located at the exit of the interferometer.
V The etalon had a spacer thickness of 2.17 mm, reflectivity in the VUV around 80%, diameter 1-inch and rms flatness of $\lambda/8$ at 200 nm.
VI Argon flow in the input and output collimators.

The etalon characteristics gave a wavelength resolution of the order of 2.1×10^{-3} nm assuming an overall finesse equal to 4. Although these characteristics were not ideal for a high resolution Fourier spectrometer, allowed the recording of the interference fringes: This was possible because the Doppler broadening of the spectral lines used was around 8×10^{-5} nm at 200 nm, and the average spectral line spread of the isotopes used was less than 10^{-5} nm. Due to the interest in having an accurate dispersion curve in the range of 5–7 eV, the combined passband of the refractometer was made to span the same range. The mechanical stability of the etalon was achieved by the kinematic mount technique described in [6,7]. We redesigned the mechanical construction in order to be adjusted in our geometry and spectral requirements. After constructing and testing several filters with various transparencies, we settled on a filter with a transparency curve peaking at 185 nm (34%) with a FWHM of 33 nm. In this way we optimised the performance of the system, since the Pt–Ne [1] lamp spectrum [8,10,11,16] has strong emission peaks at photon energies below 5 eV, and the photomultiplier used had a sensitivity extending up to 320 nm.

The spectral lines of the Pt in this lamp have extremely good coherence as has been pointed out and applied by Abjean et al. [12].

To record an interferogram, gas samples from the Barrel or Forward RICH detectors [2] are

[1] Cathodeon, part No 3QNY.

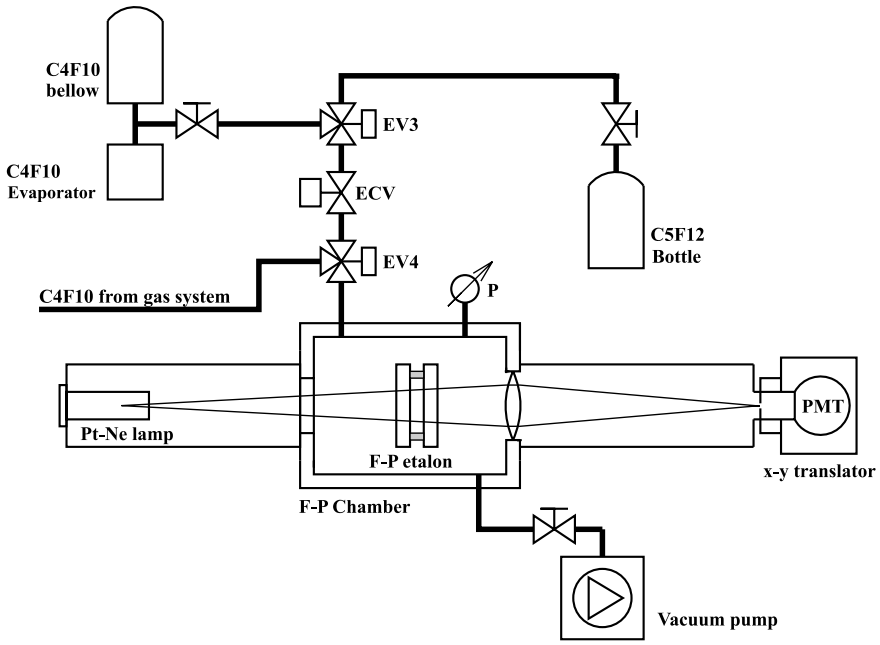

Fig. 1. A simplified diagram of the experimental setup of the refractometer. The Electronic Control Valve (ECV) is controlled by the computer, while the electro-valves EV3 and EV4 are activated electrically depending on the gas sample to be selected each time.

introduced into transfer bottles at different temperatures. The C_4F_{10} is introduced as a liquid and is evaporated under pressure up to about 2500 hPa, at the ambient temperature (~22 °C). The C_5F_{12} gas is introduced under a pressure of about 1100 hPa at a stabilised temperature of 40.0 ± 0.1 °C.

The gas flow, monitoring and control is described below. In Fig. 1 we present the schematics of the set of valves used in the refractometer and also the main optical components. In order to achieve a linear dependence of the pressure versus time during the gas sample insertion, we developed a computer program for the regulation, in real time, of the gas flow via the Electronic Control Valve (ECV). [2] The desired fraction of the ECV opening indicated by the program, was converted in a analogue voltage via a D/A card and then into a corresponding required electrical current to activate the valve mechanism [9]. The 3-way electrovalves EV3 and EV4 are activated electrically depending on the gas sample to be selected each time.

[2] MKS 248A-00100SV.

The vacuum pump is used to establish a vacuum in the Fabry–Perot chamber (better than 2 hPa) before the gas sample insertion. The linear relationship between gas pressure and time allows the uniform in time recording of interference fringes for each spectral line of the lamp.

During measurements the Fabry–Perot chamber, the piping and the bottles, are heated in order to obtain the refractivity close to the operating temperatures in the detector for each gas (32 and 40 °C respectively). Temperature controllers are used to keep the temperature within a variation of 0.1 °C from the above desired values.

3. Data analysis method

3.1. Lamp spectrum reconstruction

A quick analysis of the resulting interferometric data can be performed on the PC, which is used to control the refractometer, but for a detailed analysis the data are transferred to a workstation or a mainframe computer. The principle of the method

is described in [13] and was used in measurements obtained using samples of gas radiators [5]. In the present work we extended the method in a way that the frequency spectrum, obtained from the Finite Discrete Fourier Transform of the interferometric data, is used to reconstruct the light source (lamp) spectrum, by assuming a candidate dispersion curve for the gas refractivity.

In the reconstructed spectrum some characteristic peaks are composite, being formed by the coalescence of the neighbouring spectral lines. This is due to the finite spectral resolution of the interferometer [3]. For these peaks, the value of the refractivity is taken as the mean of the refractivities at the corresponding component wavelengths.

3.2. Simulation of the Fabry–Perot interferometer

From the great multitude of the Pt–Ne hollow cathode spectral lines found in the literature, only the ones above a certain intensity limit are selected. The 77 lines obtained are used for the subsequent simulation of the Fabry–Perot interferometer. The simulation, which includes, among the spectral line broadening mechanisms the Doppler broadening as a main contributor, is necessary in order to identify the spectral peaks where the refractivity has to be determined; furthermore, it takes into account the etalon mirror imperfections. It has been shown, by a separate study, that in this type of lamp, the effects of isotopic shift of the Pt lines on the simulated reconstructed spectrum are small, compared to the above effects, and therefore are not included in the simulation procedure. It is to be noted that after examination we concluded that the effect of hyperfine structure is negligible.

Because the intensities of each of the 77 lines are affected by the PMT spectral sensitivity and the optical filter, they are added incoherently to form a composite interferogram. It should be noted, that the intensity values found in the literature were corrected to correspond (a) to the results of the spectrum given by the manufacturer and (b) with measurements taken by our grating spectrometer; furthermore, the PMT spectral efficiency was also taken into account.

This interferogram is Fourier analyzed in order to obtain the "power spectrum" in units of fringes per unit pressure. Moderate deviation of the selected dispersion curve from the actual (unknown yet) one, does not affect the position of the peaks; it can only have some influence on their widths.

3.3. Method to extract the refractivity from an actual interferogram

Each interferometric data set is analyzed in the frequency domain to obtain the power spectrum. From the latter, the corresponding reconstructed spectrum can be extracted, by comparing the experimental and simulated spectra, and examining the matching between the two sets of peaks. A cross-correlation between the two spectra is applied to aid the identification procedure. When the optical properties of the gas radiator have been stabilised and the identification of the main peaks has been successfully performed, the above cross-correlation procedure is not necessary. Figs. 2 and 3, show a typical power spectrum and the corresponding reconstructed spectrum from analyzed interferometric data, taken with the gas radiator C_4F_{10}. The conversion of the plot presentation from frequency to wavelength is being performed using the same dispersion curve, used in the simulation procedure, as discussed in Section 3.2.

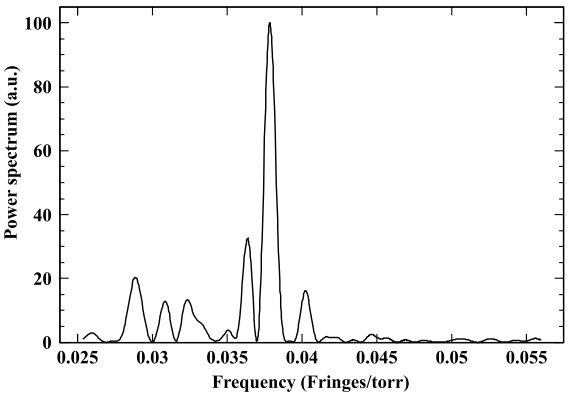

Fig. 2. A typical power spectrum of an experimental interferogram taken in June 1999 with the gas radiator C_4F_{10}, obtained from the analysis software. The r.m.s. of the noise level is of the order of 2 (a.u.) and the S/N-ratio of the dominant peak is 50.

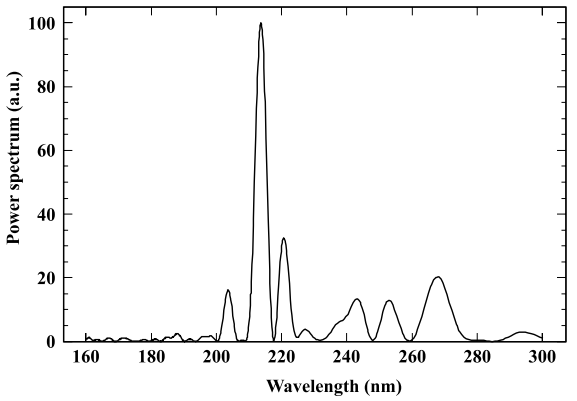

Fig. 3. The reconstructed spectrum of the above interferogram, where the wavelength is used as a variable in the x-axis instead of the frequency. The dominant peak, at 212 nm, corresponds to the simulated (actual) peak of 208.8 nm. The small difference, 3.2 nm, is explained in the text.

The dominant peak in the plots is used for the regular measurements (monitoring) of the gas refractivity, while the study of the complete set of main peaks is necessary for the extraction of the dispersion curve. The small difference of 3.2 nm between the wavelength of the experimental and the simulated peak, is mainly due to the difference between the actual dependence of refractivity on wavelength and the initially selected dispersion curve. It has been used without further change up to now.

In the following, we describe the specific steps of the calculation: For each identified peak, the corresponding wavelength λ_0 is used to determine the refractivity $n-1$, using the well known expression of the pressure tunable Fabry–Perot interferometer,

$$n(\lambda_0, P, T_0) - 1 = \frac{\lambda_0}{2d} N(\lambda_0, P, T_0), \tag{1}$$

where, d is the etalon mirror spacer thickness and N is the total number of fringes (generally fractional) over the pressure variation from zero to the final pressure P at absolute temperature T_0; N is determined by the formula

$$N(\lambda_0, P, T_0) = f_{\mathrm{av}} \Delta P, \tag{2}$$

where, f_{av} is the average frequency in units of fringes per unit pressure during the total pressure variation up to a value P. The gradual increase of the frequency during the recording of an interferogram is due to the "non-ideal gas" nature of the fluorocarbons, as explained in [13]. In the previous reference, it was discussed that, within some constraints, the quantity f_{av}, corresponds to the peak where the refractivity is being determined, according to the Woodword's theorem [14,15].

4. Estimate of the systematic errors

In determining the refractivity, we only used the quantities λ_0, f_{av}, d, and P, because, as it evident from Eqs. (1) and (2), they are the most dominant. In the following, we analyse quantitatively each of the above parameters:

To reduce the λ_0 uncertainty, we selected the Pt–Ne lamp because of its very good coherence properties in the VUV region [16]. Moreover, the resolution of the reconstructed spectrum constitutes the main role for the uncertainty of λ_0. This uncertainty can be reduced by using a wider pressure variation, with given etalon spacer thickness and gas type. Typical values, depending on the spectral range, vary from 0.5 to 1.5 nm (or about 0.3–0.8%).

The uncertainty of the "average frequency", f_{av}, is estimated from the resulting power spectrum of the specific peak and its relative accuracy is comparable to the accuracy of λ_0.

The systematic error of the etalon spacer thickness, d, is less than 0.5%. The pressure reading error is also less than 0.5% (in Full Scale, 1500 hPa). This accuracy was achieved by regular comparison of the electronic sensor reading with a near-by mercury barometer, and we re-calibrated the sensor if it was necessary. The non-linearity of the pressure sensor over the range 0–1100 hPa has been determined from the experimental data themselves to be less than 1%, but its influence on the refractivity determination has been shown to be less than 0.1% [17].

The systematic deviation of the temperature during the gas introduction is kept at less than +0.1 °C by the temperature control system. The relative statistical variations are negligible.

The overall systematic error in the determination of $n-1$, in the range 180–220 nm, has been estimated to be 1.0–1.2%.

5. Experimental results

5.1. Results with gas radiators

During the running period in 1996 we started taking some specific refractivity measurements either using optical filters, or analysing the data in various wavelengths without any filter. Our aim was to build a typical dispersion curve for each gas radiator using also some older data in the visible and UV range, with a mercury lamp as light source. These curves were useful for the data analysis, as we mentioned in Section 3. The data were fitted using the well-known Sellmeier equation,

$$(n-1) = \frac{10^{-6} p_1}{p_2^{-2} - \lambda^{-2}}, \tag{3}$$

where, λ is the wavelength in nm and p_1 and p_2 are the fit parameters to be determined.

The values of the fitted parameters are: $p_1 = 0.1890\ \text{nm}^{-2}$, $p_2 = 86.57$ nm for C_5F_{12} and $p_1 = 0.2320\ \text{nm}^{-2}$, $p_2 = 73.63$ nm for C_4F_{10}. In Figs. 4 and 5 we show for comparison the fitted dispersion curves of C_5F_{12} and C_4F_{10}, respectively, measured during the 1996 and 1999 run periods. In these plots, the error bars along the wavelength axis represent the finite resolution in identifying the particular spectral peak (the resulting peak from the contribution of the neighbourhood spectral lines). The resolution varies from about 1.5–4 to 1.8–5 nm, respectively. The error bars along the refractivity axis vary in value and represent the systematic error from one measurement.

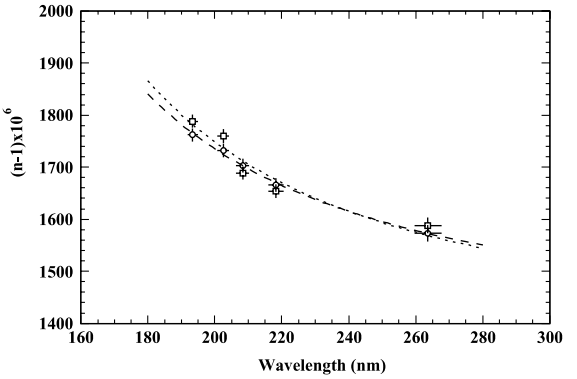

Fig. 4. The fitted dispersion curves of C_5F_{12} based on experimental data taken during 1996 (open circles) and 1999 (open squares) run periods.

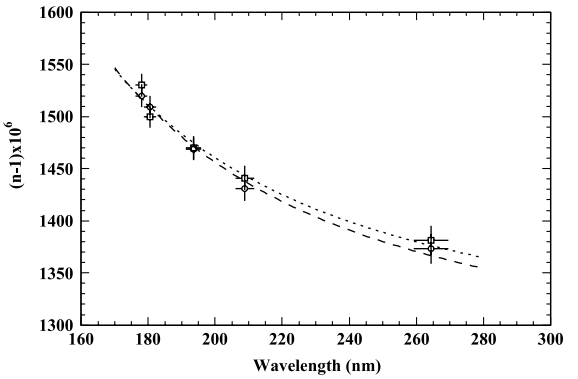

Fig. 5. The fitted dispersion curves of C_4F_{10} based on experimental data taken during 1996 (open circles) and 1999 (open squares) run periods.

We decided to monitor the refractivities of C_5F_{12} and C_4F_{10} at 208.8 and 208.3 nm, respectively, because of the highest peak intensity and good repeatability in detecting these peaks. The resulting refractivities are linearly extrapolated to 1030 hPa and registered in the database, in both cases. Results at other wavelengths are also extracted for comparison.

The experimentally determined values of C_5F_{12} and C_4F_{10} refractivities during the 1996–1999 period, measured by the DELPHI refractometer, are also shown in Table 1, and the plots of the evolution are shown in Figs. 6–8.

We fitted each data set by a second-degree polynomial, in order to study the statistical and systematic variations. The "reduced chi-square" (χ^2/n) of the fit was 0.47 ($n = 12$, CL = 90%) and 1.5 ($n = 14$, CL = 10%) respectively, and thus, the fits are acceptable. The uncertainties of the refractivity, due to the errors of the fit parameters, are $\delta n_{\text{stat}} = 23$ and $\delta n_{\text{stat}} = 7.4$ respectively. In order to extract definite conclusions on the stability of the fluid systems, we also examined the existence of the systematic variations during the monitoring period. Indeed, a slight drop of the refractivity is

Table 1
The resulting refractivity values of gas radiators

Refractivity results					
C_5F_{12}			C_4F_{10}		
Week number	$(n-1)\times 10^6$ at 208.3 nm	$\delta n \times 10^6$	Week number	$(n-1)\times 10^6$ at 208.3 nm	$\delta n \times 10^6$
47	1687	15	23	1439	13
49	1707	15	30	1436	13
50	1703	15	47	1428	13
87	1700	15	86	1458	13
88	1708	15	87	1459	13
89	1722	15	88	1457	13
91	1694	15	91	1424	13
118	1703	15	93	1431	13
128	1688	15	127	1438	13
134	1699	15	141	1405	13
146	1700	15	146	1420	13
148	1680	15	148	1405	13
187	1681	15	172	1425	13
192	1686	15	181	1410	13
196	1695	15	187	1427	13
			191	1426	13
			196	1439	13

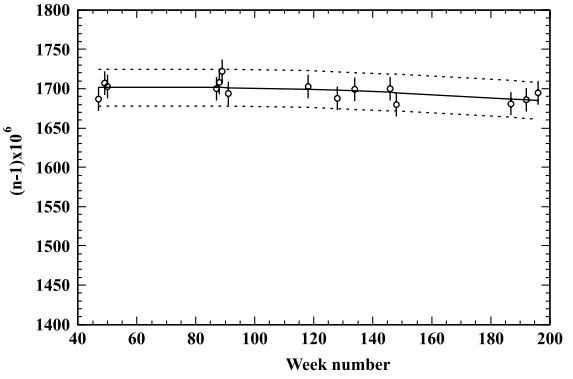

Fig. 6. The fitted curve (solid line) of the refractivity evolution of the gas radiator C_5F_{12}. The zone between the dotted lines represents the parameter uncertainty from the fit. The experimental values corresponds to the conditions $P = 1030$ hPa and $\theta = 40$ °C at 208.3 nm, with an average value of 1997.

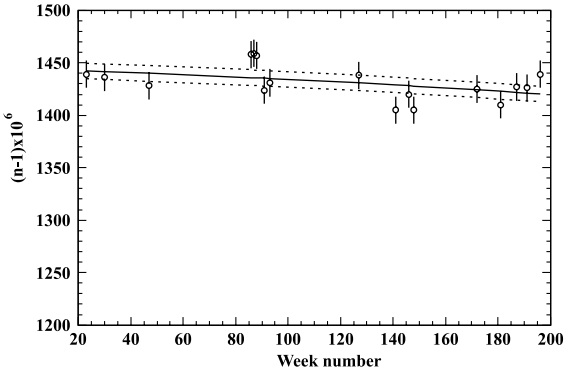

Fig. 7. The fitted curve (solid line) of the refractivity evolution of the gas radiator C_4F_{10}. The zone between the dotted lines represents the parameter uncertainty from the fit. The experimental values corresponds to the conditions $P = 1030$ hPa and $\theta = 32$ °C at 208.8 nm, with an average value of 1431.

observed causing a total difference $\delta n_{sys} = 17$ and $\delta n_{sys} = 22$ respectively. In the case of C_5F_{12} the systematic variation is not detectable because $\delta n_{sys} \sim \delta n_{stat}$, while in the case of C_4F_{10}, $\delta n_{sys} = 3\delta n_{stat}$ and we can infer the existence of a total systematic variation of $(-1.5 \pm 0.5)\%$. These results lead to the conclusion, that the stability of the fluid system was very high: i.e. within statistical variations of about 1.4 and 0.5% respectively.

Because we suspected that the C_5F_{12} was contaminated with nitrogen, we measured the refractivity at the inlet, and compared it with a sample at the outlet of the Barrel RICH detector. The measurements were used to extract the information on

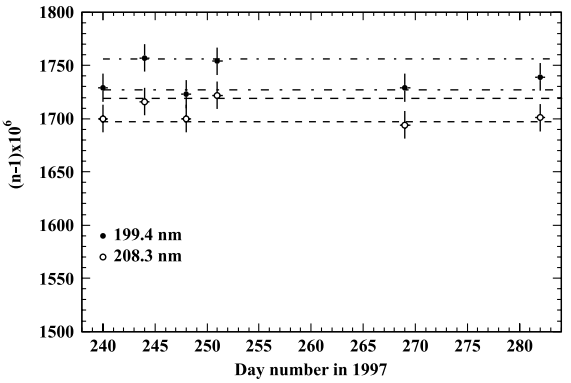

Fig. 8. Specific measurements of gas radiator C_5F_{12} from inlet and outlet of Barrel RICH detector at two wavelengths in VUV. The dashed lines represent the average value in both cases.

the average percentage of the nitrogen inside the gas radiator of the detector. In order to achieve higher reliability, we determined the refractivity at two particular spectral peaks (199.4 and 208.3 nm), under the same conditions, in a period of 11 days. The results were also compared with two subsequent measurements at the output of the Barrel RICH (see Fig. 8).

Using experimental values of the nitrogen refractivity at the spectral region of interest [18], we measured a difference of $(1.40 \pm 0.4)\%$ in $n-1$, near the VUV region, between inlet and outlet.

If we assume a binary mixture (C_5F_{12}–N_2), the percentage of Nitrogen to account for this difference, is extracted from the following formula:

$$x_{N_2} = \frac{n_o - n_i}{n_{N_2} - n_i}, \tag{4}$$

where n_i, n_o are the refractive indices of C_5F_{12} in the inlet and outlet respectively, extrapolated to the wavelength of 185 nm by using the fitted dispersion curve. Also, n_{N_2} is the refractive index of Nitrogen at (1030 hPa/40 °C, 184 nm). The computed percentage was $(1.7 \pm 0.4)\%$.

5.2. Measurements with vapours of the liquid radiator

During normal operation, small quantities of vapour of the liquid radiator C_6F_{14} get mixed with the pure gas radiator C_5F_{12} inside the Barrel RICH detector. As a result, the overall refractivity of the binary mixture (C_5F_{12}/C_6F_{14}) is slightly higher than the one coming from the gas radiator alone. The composition of the radiator fluids in terms of the C_5F_{12}/C_6F_{14} mixing ratio and also its nitrogen content have been monitored by a vapour pressure cell analysis [19]. The purity of the liquids at the input of the radiator systems, i.e. before mixing due to leaks has taken place, are measured at a distillation plant. The above systems give useful information and assure the desired stability of the fluid radiators.

To determine the refractivity of the C_5F_{12}/C_6F_{14} binary mixture, contaminated with nitrogen, we found it necessary to perform a specific measurement of the refractivity of the pure C_6F_{14} in its gas phase. This was accomplished for the first time, during normal operation, by introducing a certain volume of vapours of the liquid radiator C_6F_{14} into the refractometer, using the same bottle as for C_5F_{12} but under 45 °C and 667 hPa. The value of $n-1$ was determined at two particular wavelengths, 200.5 and 208.3 nm. The measured values, extrapolated to 1030 hPa and 40 °C, are presented in Table 2. In this extrapolation we assumed a linear dependence of refractivity on pressure. These values, and the determined mixing ratio of the nitrogen, mentioned above, lead to an expected refractivity value of C_5F_{12} in the output of the Barrel RICH, consistent with that obtained experimentally using the refractometer, during the operation of the Barrel RICH detector.

Additionally, a good consistency with our own measurements of C_6F_{14} refractivity in liquid form, extrapolated to the gas phase, has been found (see Ref. [20,21]).

Table 2
The resulting refractivity results with liquid radiator C_6F_{14} in gas phase (δn represents the overall error)

Results with vapours of the liquid radiator			
λ (nm)	$\delta\lambda$ (nm)	$n-1$ ($\times 10^6$)	δn ($\times 10^6$)
200.5	1.5	2200	30
208.3	1.5	2040	30

6. Conclusions and prospects

The capabilities and performance of the DELPHI RICH refractometer, operating near the VUV region for 4 years are presented. The extracted data lead to the conclusion that the stability of fluids during the above period is very high (with a RMS statistical variation of less than 1%), as seen by the evolution of the refractive index in the wavelength range of interest for either Barrel or Forward RICH. A small drop of the $n-1$ value, observed for C_4F_{10} during these 4 years, was about -22×10^{-6} (i.e. less than twice the systematic experimental error of the refractometer).

Also for the first time, the refractivity of the liquid radiator C_6F_{14} in gas phase has been measured as well. It was found that the corresponding influence on the refractivity of the Barrel RICH radiator was comparable to the one expected from its small mixing ratio.

Small variations in the gas refractivity (down to $\sim$0.5%) can be detected by the refractometer, due to its high enough sensitivity, as explained in Section 3.2. Although the refractometer operated in a harsh environment due to the presence of mechanical vibrations, it has reached, during the last 4 years, a level of stable operation. It can give valuable information on the optical quality of the RICH radiator fluids.

In short, we have presented a flexible, easily installed system, with minimum operational cost and high efficiency, which can monitor refractivities of gases, giving values comparable in accuracy to more elaborate and expensive systems. A similar apparatus could be used in some future High Energy experiments which use the RICH technique.

Acknowledgements

The authors would like to greatly acknowledge the cooperation of Valerio Gracco, Olav Ullaland, Christian Joram, George Lenzen and H. Rahmani on the development and evaluation of the performance of the DELPHI refractometer and also E. Albrecht and P. Carrie for their support during the refractometer operation.

References

[1] J. Seguinot, T. Ypsilantis, Nucl. Instr. and Meth. 142 (1977) 377.
[2] E. Albrecht et al., Nucl. Instr. and Meth. A 433 (1999) 47.
[3] J.M. Vaughan, M.A. DPhil, The Fabry–Perot Interferometer.
[4] E. Fokitis, S. Maltezos, K. Patrinos, Nucl. Phys. B 44 (Proc. Suppl.) (1995) 246.
[5] A. Filippas, E. Fokitis, S. Maltezos, K. Patrinos, Nucl. Instr. and Meth. A 371 (1996) 255.
[6] D. Rees, T.J. Fuller-Rowell, A. Lyons, T.L. Killeen, P.B. Hays, Appl. Opt. 21 (21) (1982) 3896.
[7] T.L. Killeen, P.B. Hays, B.C. Kennedy, D. Rees, Appl. Opt. 21 (1982) 3903.
[8] J.Z. Klose, G.F. Hartig, W.J. Rosenberg, Appl. Opt. 29 (19) (1990) 2951.
[9] S. Maltezos, Control Systems for the Experimental Setups of the DELPHI Detector Ph.D thesis (unpublished) (1996) 100.
[10] G.H. Mount, G. Yamasaki, W. Fowler, W.G. Fastie, Appl. Opt. 16 (1977) 591.
[11] P.G. Wilkinson, K.L. Andrew, J. Opt. Soc. Am. 53 (1963) 710.
[12] R. Abjean, A. Bideau-Mehu, Y. Guern, Nucl. Instr. and Meth. A 292 (1990) 593.
[13] S. Maltezos, A. Filippas, E. Fokitis, DELPHI Note 96-95 RICH 87 (1996).
[14] P.M. Woodward, Telecommunications Research Establishment, Great Malvern, Worcs., England, Memo. 666 (1952).
[15] N.M. Blachman, G. McAlpine, IEEE Trans. Commun. Technol. com-17 (2) (1969) 201.
[16] S. Bouazza, J. Bauche, J. Opt. Soc. Am. 10 (1988) 1.
[17] K. Patrinos, Experimental Study of Refractive Indices of Gas Radiators of the DELPHI RICH Detectors using Piezotunable Fabry–Perot Interferometer, Ph.D thesis (unpublished) (1999) 110.
[18] P.W. Langhoft, M. Karplus, J. Opt. Soc. Am. 59 (7) (1969) 863.
[19] C. Joram, M.J. Tobar, DELPHI Note 98-36 RICH 93 (1998).
[20] P. Moyssides, S. Maltezos, E. Fokitis, J. Mod. Opt. 47 (10) (2000) 1693.
[21] CERN/LHCC 98-19 ALICE TDR 1 (1998) 35.